Simulation of Oxide Trapping Noise in Submicron n-Channel MOSFETs

Fan-Chi Hou, Gijs Bosman, and Mark E. Law, *Fellow, IEEE*

***Abstract*— Carrier trapping via tunneling into the gate oxide was implemented into a partial differential equation -based semiconductor device simulator to analyze the $1/f$-like noise in silicon MOSFETs. Local noise sources are calculated using the carrier tunneling rates between trap centers in the oxide and those at the interface. Using the Green's transfer function approach, noise contributions from each node in the oxide mesh to the overall noise at the specified contact terminals are simulated. Unlike traditional $1/f$ noise analyses in MOSFETs, the simulator is capable of simulating noise for a wide range of bias voltages and device structures. The simulation results show that for an uniformly doped channel, the region in the oxide above the pinch-off point in saturation is most critical for low frequency noise generation while for a graded channel device the source side of the gate oxide region becomes important. By comparing the simulation results with the measured noise data, the oxide defect density in the noise producing regions can be profiled.**

***Index Terms*— Carrier trapping, semiconductor defects, semiconductor device noise.**

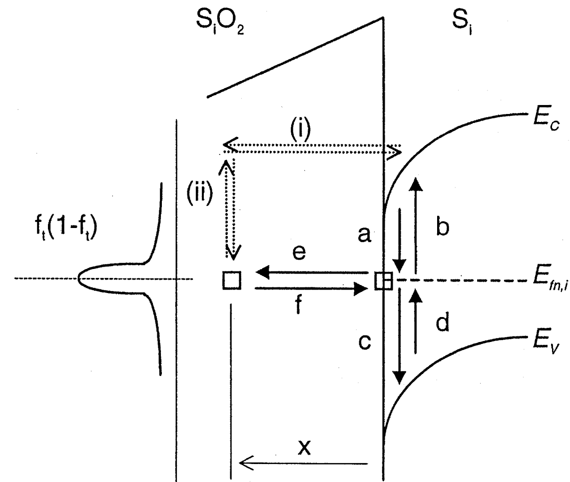

Fig. 1. "Tunneling and Capture (i,ii)" and "Capture and Tunneling (a–f)" models. The arrows indicate electron transitions.

I. Introduction

THE $1/f$-like noise in silicon devices has been studied extensively in the past. Most evidence has shown that its sources are located at or near Si/SiO_2 interfaces. This partially explains the fact that $1/f$-like noise is more dominant in MOS devices than in bipolar transistors, due to MOS structures having larger surface areas in critical device regions. According to McWhorter and others [1]–[5], $1/f$-like noise is the superposition of different Lorentzian spectra of which the corner frequencies spread across the low-frequency spectral window. The corresponding characteristic time τ of each Lorentzian spectrum, calculated from its corner frequency, gives information on the tunneling between defect centers in the oxide and at the interface. Even though the carrier tunneling mechanism between the traps in the oxide and at the interface is the source of $1/f$-like noise, only its macroscopic effect, represented by a characteristic time τ, is used in analytical derivations. Typically, deriving the $1/f$-like noise spectral density from carrier tunneling equations and microscopic generation-recombination $(g - r)$ noise sources in actual devices operating under bias is difficult due to the complexity of the problem. In recent years, device noise simulation packages have been implemented successfully into partial differential equation (PDE) -based device simulators. Utilizing the vector and scalar Green's functions calculated by the simulators, the noise at device terminals from each local noise source can be calculated. Simulations of diffusion, Hooge $1/f$, and bulk $g - r$ noise have shown that none of these mechanisms can produce $1/f$-like noise in MOS devices [6]. The focus of this paper is on surface noise, or so-called oxide trapping noise, simulations. The difficulty with the simulation of carrier tunneling mechanisms and oxide trapping noise is that carrier tunneling is not just dependent on variables at local grid points and adjacent points, but also depends on variables at grid points that are distant. The noise simulator needs to generate and use a database to keep track of the link between each oxide point and its corresponding interface point. FLOODS (FLorida Object-Oriented Device Simulator) [7], [8] was used as a platform for our simulation studies.

II. Theory and Implementation

As stated previously, McWhorter's theory has been used frequently to explain the $1/f$ noise in MOS devices. Christensson [2] and others proposed a "Tunneling and Capture" model, in which (i) the carriers first tunnel to a distance from the continuum states at the interface into the oxide, and then (ii) are captured by traps that have the same energy as E_f. This model is illustrated in Fig. 1. The validity of this model was later questioned, since measurement data did not support energy dissipation in the oxide [9]. The "Capture and Tunneling" model was proposed by Fu and Sah [4] as an alternative to the previous

Manuscript received July 15, 2002; revised December 12, 2002. The review of this paper was arranged by Editor M. J. Deen.

The authors are with the Department of Electrical and Computer Engineering, University of Florida, Gainesville, FL 32611 USA (e-mail: bosman@ece.ufl.edu; law@tec.ufl.edu).

Digital Object Identifier 10.1109/TED.2003.811395

0018-9383/03$17.00 © 2003 IEEE

proposed model. In the latter, the carriers first get trapped by fast defect centers at the interface through a Shockley-Read-Hall (SRH) process, indicated as processes a, b, c and d in Fig. 1, and then tunnel into the traps in the oxide, illustrated as processes e and f. Thus the carriers do not dissipate energy in the oxide. A continuous trap energy distribution over the bandgap at the interface is required for this process to be effective, the presence of which is generally accepted for the SiO_2/Si interface system. Fu and Sah's "Capture and Tunneling" model is used as the basis for the oxide trapping mechanism implemented in our simulation study.

A. "Capture and Tunneling" Model

Fig. 1 shows the energy band diagram that illustrates the possible carrier transition processes at the interface and in the oxide [4]. Carriers in the continuum states can get trapped (process a & c) or de-trapped (process b & d) from the localized defect centers at the interface, through the SRH process. The arrows indicate electron transitions. The trapped carriers can also communicate with defect centers that have the same energy in the oxide through tunneling (process e & f). Since the trap centers at the interface and in the oxide are distributed in energy and space, discretization in both variables is needed. Measured data in the past [10] generally describes the trap distribution per unit of energy and volume as U-shaped in energy. Thus, it may be modeled as [5], [11]

$$N_t(E) = N_0 \exp\left[\xi |E - E_i|\right]. \tag{1}$$

The term E_i is the intrinsic energy level, ξ a fitting parameter, and N_0 the trap density at midgap. Discretization in small energy intervals would require a large number of trap electron continuity equations to be specified to the system. Thus carefully choosing the discretization scheme for noise simulation is critical. According to $g-r$ noise theory, the power spectral density due to a fluctuation in the density of trapped carriers n_t in a differential volume $\Delta\Lambda$ is [2], [5], [12]

$$S_{\Delta\Lambda n_t} = \frac{4\tau}{1+\omega^2\tau^2} N_t f_t \frac{(1-f_t)}{\Delta\Lambda} \tag{2}$$

where τ is the trapping time constant and f_t is the Fermi-Dirac distribution function. Plotting the function $f_t(1-f_t)$, which is a strong function of energy E, will display the critical energy levels where the contributions of the $g-r$ noise are predominantly coming from. As shown in Fig. 1, this function is most significant at the electron quasi-Fermi level at the interface $E_{fn,i}$. This allows us to focus on the trap levels at $E_{fn,i}$ only with an effective trap volume density $N_t' = 4kTN_t(E_{fn,i})$. For the effective trap levels at $E_{fn,i}$, the Shockley densities are equal to

$$n_1 = n_i \exp\left[\frac{(E_f - E_i)}{kT}\right] = n \tag{3}$$

$$p_1 = n_i \exp\left[\frac{(E_i - E_f)}{kT}\right] = p. \tag{4}$$

The rate equations characterizing the processes a, b, c, and d in Fig. 1 then become

$$\begin{aligned} r_{n,\text{int}} &= c_n n\,(N_t' - n_t) = c_n n\left[4kTN_0 e^{\xi(E_f - E_i)} - n_t\right] \\ &= c_n n\left[4kTN_0\left(\frac{n}{n_i}\right)^{\xi kT} - n_t\right] \end{aligned} \tag{5}$$

$$g_{n,\text{int}} = c_n n_1 n_t = c_n n n_t \tag{6}$$

$$r_{p,\text{int}} = c_p p n_t \tag{7}$$

$$\begin{aligned} g_{p,\text{int}} &= c_p p_1\,(N_t' - n_t) = c_p p_1\left[4kTN_0 e^{\xi(E_f - E_i)} - n_t\right] \\ &= c_p p\left[4kTN_0\left(\frac{n}{n_i}\right)^{\xi kT} - n_t\right] \end{aligned} \tag{8}$$

respectively. The basic equations for the discretized energy level at the interface become

$$\begin{aligned} F_\psi = &-\frac{d^2\psi}{dr^2} \\ &-\frac{q}{\varepsilon}\left[p - n + N_D^+ - N_A^- - Q_{itf}(E_f)/q - n_{t,itf}\right] \\ =&0 \end{aligned} \tag{9}$$

$$\begin{aligned} F_n =& \frac{dn}{dt} - \frac{1}{q}\nabla\cdot\boldsymbol{J}_n + (r_{n,itf} - g_{n,itf}) \\ &- \gamma_{n,itf}(\boldsymbol{r}, t, E_f) = 0 \end{aligned} \tag{10}$$

$$\begin{aligned} F_p =& \frac{dp}{dt} + \frac{1}{q}\nabla\cdot\boldsymbol{J}_p + (r_{p,itf} - g_{p,itf}) \\ &- \gamma_{p,itf}(\boldsymbol{r}, t, E_f) = 0 \end{aligned} \tag{11}$$

$$\begin{aligned} F_{n_t,\text{int}} =& \frac{dn_{t,itf}}{dt} + (g_{n,itf} - r_{n,itf}) \\ &- (g_{p,itf} - r_{p,itf}) - \gamma_{t,itf}(\boldsymbol{r}, t, E_f) \\ &- (g_{ox} + r_{ox}) - \gamma_{ox}(\boldsymbol{r}, t, E_f) = 0 \end{aligned} \tag{12}$$

where $\gamma_{n,itf}$, $\gamma_{p,itf}$, and $\gamma_{t,itf}$ are the Langevin noise terms describing random transition rate fluctuations at the interface, and γ_{ox} is the Langevin noise term associated with transition rate fluctuations in carrier tunneling. The terms r_{ox} and g_{ox} are the tunneling rates illustrated as processes e and f in Fig. 1, respectively. These tunneling rates are functions of the tunneling coefficient T, the trapped carrier density of the defect centers in the oxide $n_{t,ox}$, and the trapped carrier density of the defect centers at the corresponding interface node $n_{t,itf}$

$$r_{ox}(x_i) = T n_{t,\text{int}}(N_{t,ox} - n_{t,ox})\Delta x \tag{13}$$

$$g_{ox}(x_i) = T(N_{t,\text{int}} - n_{t,\text{int}}) n_{t,ox}\Delta x. \tag{14}$$

Notice that these rate equations do not only dependent on the local variables at the oxide node, but also dependent on the variables at the interface. In addition, the tunneling coefficient T in units of cm^2/s varies with the distance between each pair of nodes that the carriers tunnel between.

For each oxide node the Poisson and trap electron continuity equations need to be included as

$$\begin{aligned} F_{\psi_{x_i}} =& -\frac{d^2\psi_{x_i}}{dr^2} - \frac{q}{\varepsilon}\left[-\frac{Q_{ox}(x_i, E_f)}{q} - n_{ox}(x_i, E_f)\right] \\ =&0 \end{aligned} \tag{15}$$

$$\begin{aligned} F_{ox} =& \frac{dn_{ox}(x_i, E_f)}{dt} - r_{ox} + g_{ox} - \gamma_{ox}(x_i, t, E_f) \\ =&0. \end{aligned} \tag{16}$$

B. Modeling of the Defect Density in the Oxide

Knowledge of the defect density distribution in the oxide is critical for understanding the operation of a MOSFET, since defects play an important role in the gate leakage current and act as the sources of low frequency noise. Any model for the oxide defect density N_t can be applied to the simulator and by comparing simulated with measured data, an optimal defect density profile can be obtained via reverse engineering. Past research [10] shows that N_t varies in position and energy. Celik and Hsiang [11] observed from n-channel MOSFETs operating in strong inversion,

$$N_t(E,x) = N_0 \exp\left[\xi(E-E_i) + \frac{q\lambda(V_g - V)x}{t_{ox}} + \eta x\right] \tag{17}$$

where N_0 is the trap density at midgap in the oxide, x represents distance into the oxide, and ξ is a fitting parameter that describes the curvature of a U-shaped distribution of the defect density in energy. The first term in the exponent is from (1). The absolute sign is no longer required since the Fermi level E_F and thus the level E of interest is greater than the intrinsic level E_I in our simulation of n-channel devices. Equation (17) assumes the same U-shaped distribution in energy at the interface and in the oxide, but shifted by band bending as modeled by the second term in the exponent where t_{ox} is the oxide thickness and V_g and V are the voltage at the gate terminal and in the channel, respectively, and λ is a fitting parameter. The parameter η accounts for a possible exponential variation in defect density near the interface. From noise measurements on MOS devices, Celik and Hsiang extracted $N_0 = 4 \cdot 10^{17}$ cm^{-1}eV^{-1}, $\xi = 3.1$ eV^{-1}, $\lambda = 62$ eV^{-1}, and $\eta = 4.5 \cdot 10^7$ cm^{-1}. Ideally, the shift of the U-shape distribution at an oxide node located at x_i should equal the exact amount of the band bending at x_i. That is, $q\lambda(V_g - V)x/t_{ox}$ can be written as $q\xi[\phi itf - \phi_{ox}(x_i)]$, where $q\phi_{itf}$ and $q\phi_{ox}(x_i)$ are the barrier heights at the interface and at the oxide node located at x_i, respectively, and $q[\phi_{itf} - \phi_{ox}(x_i)]$ is the amount of the band bending at x_i. Equation (17) thus becomes

$$N_t(E,x) = N_0 \exp\left[\xi\left(E - E_i + q\left[\phi_{itf} - \phi_{ox}(x)\right]\right) + \eta x\right]. \tag{18}$$

The effect of η for noise at low frequencies is negligible. The value of ξ can be obtained independently from various defect density extraction techniques. Thus, the only parameter that needs to be modeled or extracted is N_0 in the oxide. For the remainder of this paper, the parameter values used in the simulations are $\xi = 3.1$ eV^{-1} and $\eta = 0$.

C. Modeling of the Carrier Tunneling Rate

In general, the carrier tunneling rate is given by [2], [4], [9], [11], [13]

$$T = T_0 \exp(\alpha x) \tag{19}$$

where the attenuation constant α of the wave function depends on the shape of the barrier. It also depends on the effective mass of the carrier in the oxide m_{ox}, and the barrier height at the interface $q\phi_{itf}$. As derived by Fu and Sah [4], the tunneling rate T is related to the trapping characteristic time τ by $\tau = \tau_0 \exp(-\alpha x) \approx [TN_t(x=0)]^{-1}$ for interface traps at E_F. Thus, the tunneling coefficient T_0 is approximately equal to $1/\tau_0 N_t(x=0)$, where τ_0 is of the order of 10^{-10} s. [5] and N_t varies along the channel. There are two models that can be used to characterize carrier tunneling. The simplest one is the square barrier tunneling (SBT) model. As the name implies, the model assumes that the carrier sees a square potential barrier before tunneling. Of course this is only true under flat-band condition. Due to the simplicity of the SBT model, it is widely used as an approximation for calculating the tunneling characteristic time constant in analytical derivations of noise spectral densities. In this model, the attenuation constant is defined as

$$\alpha = -\frac{2}{\hbar}\sqrt{2qm_{ox}\phi_{itf}}. \tag{20}$$

Setting $m_{ox} = 0.4m_0$ as obtained from BSIM's parameter set [14], α is then equal to $1.303 \cdot 10^8$ cm^{-1} with $q\phi_{itf} = 4.05$ eV. In the actual simulation α will not be a constant, since it is a function of the barrier height $q\phi_{itf}$ which depends on the position of the Fermi level. In the second model the tunneling barrier is assumed to be trapezoidal [15], [16], a situation found in MOSFETs. To calculate α, both the barrier heights at the interface $q\phi_{itf}$ and at the trap location in the oxide $a\phi_{ox}$ are required, as stated in the following expression:

$$\alpha = -\frac{4}{3}\frac{\sqrt{2qm_{ox}}}{\hbar}\frac{\phi_{itf}^{3/2} - \phi_{ox}^{3/2}}{(\phi_{itf} - \phi_{ox})}. \tag{21}$$

As $\phi_{itf} - \phi_{ox}$ approach zero, the value of α in (21) approaches the one in (20). As mentioned previously, the tunneling rate equations specified in (13) and (14) rely on nonlocal variables. Carrier tunneling rates are highly dependent on the tunneling probability, which is an decreasing exponential function of distance. We therefore assume that the traps at an oxide node are most likely to interact with traps at their closest interface node. Thus a table was generated to inform the simulator which interface nodes and oxide nodes were linked for tunneling. The components of the Jacobian matrix can then be modified as follows:

$$J = \begin{bmatrix} & \vdots & & \vdots & \\ \cdots & \frac{dF(n_{ox})}{dn_{ox}} & \cdots & \frac{dF(n_{ox})}{dn_{itf}} & \cdots \\ & \vdots & & \vdots & \\ \cdots & \frac{dF(n_{itf})}{dn_{ox}} & \cdots & \frac{dF(n_{itf})}{dn_{itf}} & \cdots \\ & \vdots & & \vdots & \end{bmatrix}. \tag{22}$$

III. Comparison With Analytical Predictions

To illustrate the oxide trapping noise simulation package implemented in FLOODS, a 0.4 μm n-channel MOSFET structure with a gate oxide thickness of 89 Å was chosen for testing. As a first step the noise simulation is compared with the analytical expression for $1/f$ noise in MOSFETs to determine the accuracy of the simulation tool. In FLOODS, the oxide defect density can be specified in the form of (17) or (18). Thus, if the FLOODS input parameters for noise simulation are properly adjusted to include only the physics that was considered in Celik and Hsiang's [5] derivation, comparisons between the

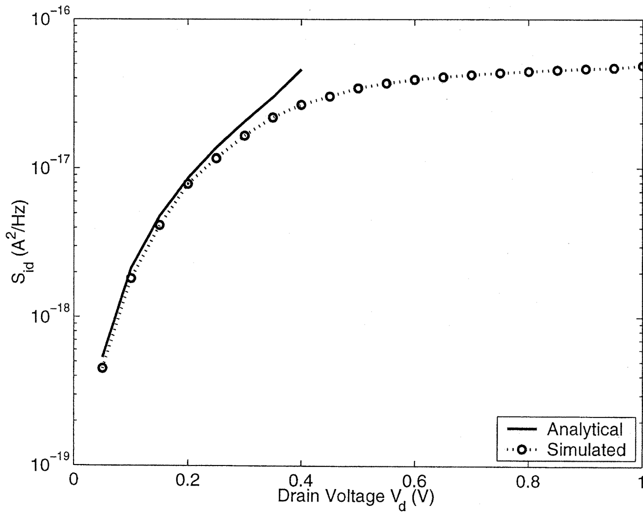

Fig. 2. Comparison of simulated and analytical noise spectral densities at $V_{gs} = 1.0$ V.

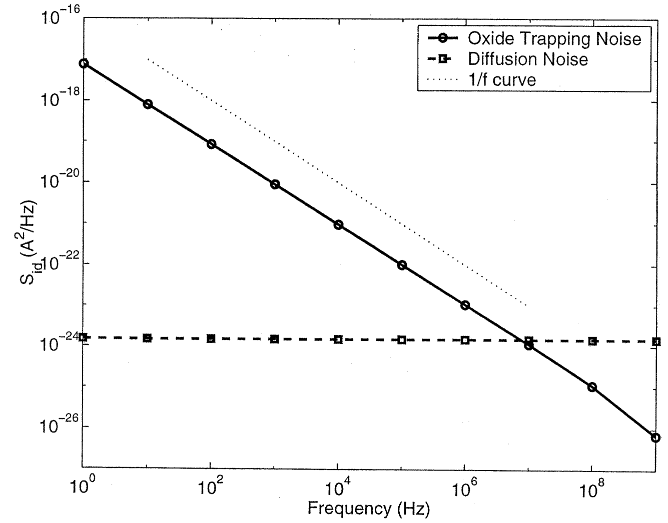

Fig. 3. Current noise spectral density at $V_{gs} = 1.0$ V and $V_{ds} = 0.2$ V.

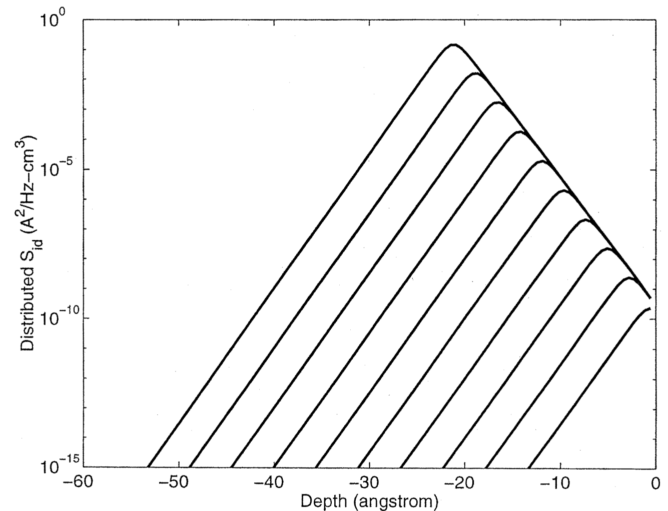

Fig. 4. Distributed current noise spectral density for different frequencies a decade apart in the gate oxide above the channel. The first curve from the left represents the 1 Hz contribution. The axis labeled "depth" is in the direction perpendicular to the oxide-silicon interface.

FLOODS simulation outcome and their analytical predictions can be made. With the assumption of an oxide defect density $N_t(E,x) = N_0 \exp[\xi|E - E_i|]$ and a square barrier tunneling model to characterize the transition of carriers between the traps at the interface and in the oxide, the current noise spectral density at the drain terminal for the linear regime of operation can be expressed as [5]

$$S_{I_d} = \frac{W\mu^2 q^2 kTN_0}{2L^3\alpha f\gamma}\left(\frac{n_{0_s}}{n_i}\right)^{\gamma} V_d(2V_{d,sat} - V_d) \times \left[1 - \frac{(V_{d,sat} - V_d)^{\gamma}}{V_{d,sat}^{\gamma}}\right] \quad (23)$$

where $V_{d,sat} = V_{gs} - V_T$, $\gamma = \xi kT$, and n_{0_s} is the surface electron concentration at the source. Equation (23) and simulation results are plotted in Fig. 2 as a function of V_d and excellent agreement is obtained for the data in the linear regime. The $1/f$ noise can be calculated analytically for the MOS device operating in the linear mode of operation only since the analytical transfer function for coupling the noise from each local noise source to the drain terminal was derived using the gradual channel approximation (GCA) and a one-dimensional description. Also, strong inversion is assumed. Therefore, the analytical $1/f$ noise formulation breaks down in saturation and in subthreshold operating regions. This is not the case when it is simulated in the PDE-based simulator, where the proper transfer function can be computed numerically at each grid point, in either the subthreshold, linear, or saturation modes of operation. At low drain bias, noise simulations were performed as a function of frequency. The results are plotted in Fig. 3. As expected, the oxide-trapping noise with the oxide trap density modeled by (17) shows pure $1/f$ noise with a corner frequency in the MHz range.

Taking a cross-section of the distributed current noise spectral densities of the oxide trapping noise at a point half way between the drain and source regions, data obtained at each frequency point, a decade apart, is plotted in Fig. 4 as a function of depth into the oxide. This figure shows that the distributed noise contributions at the lowest frequency (1 Hz), represented by the first line from the left, peaks around 22 Å away from the interface. At the next frequency (10 Hz), the overall magnitude of the current noise spectral density decreases and the peak moves closer to the interface. From this figure, one can identify the critical noise region at any specific frequency and determine how far it is away from the interface.

As stated previously, a square-barrier tunneling model with a defect density distribution independent of spatial position is used for comparison. In this model the tunneling rates and the corresponding characteristic times depend only on distance. Thus, the critical distance d_{crit} depends uniquely on the frequency of the spectral component under study. From the example in Fig. 4, $d_{\text{crit}}(1 \text{ Hz}) = 22$ Å. The distributed current noise spectral density stemming from sources in the oxide and calculated at the drain terminal (for the entire gate oxide region) is plotted in Fig. 5, to illustrate that the noise contributions for a specific frequency f $(= 1 \text{ Hz})$ maximize at the distance d_{crit} $(= 22$ Å$)$ away from the interface along the channel.

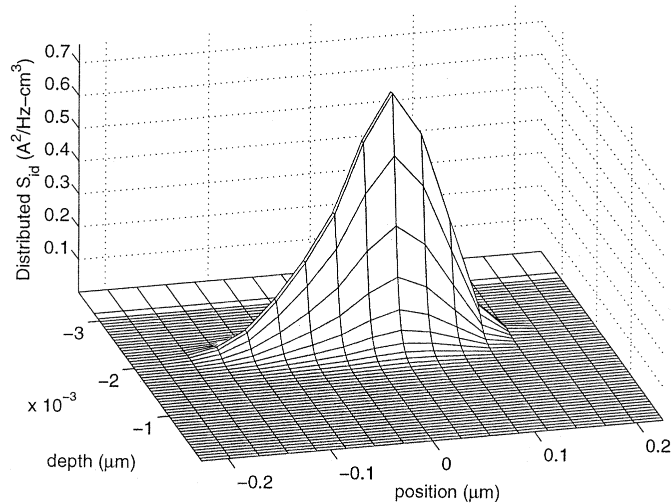

Fig. 5. Distributed current noise spectral density along the channel at $V_{gs} = 1.0$ V and $V_{ds} = 0.45$ V for a spectral component at $f = 1$ Hz. The axis "position" is parallel to the channel, and its origin is midway between the metallurgical source and drain junctions. The source and drain metallurgical junctions are located at ± 0.2 μm.

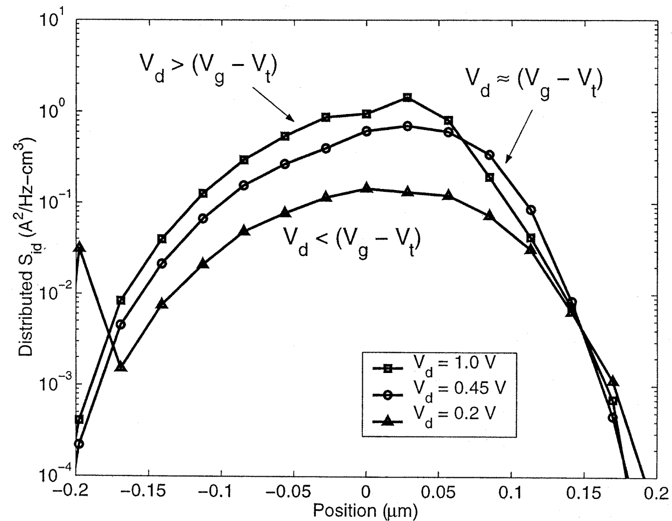

Fig. 6. Distributed current noise spectral density along the channel for different bias conditions.

To observe the changes in oxide trapping noise in different regimes of device operation, the cross-section of the distributed current noise spectral density parallel to the channel, taken at the critical distance d_{crit} away from the interface, is plotted under different drain bias conditions in Fig. 6. In the linear mode of operation, noise contributions of each oxide section parallel to the channel increase as V_{ds} increases. As the drain bias increases beyond $V_{d,sat}$, the peak of the ridge shifts toward the source, the same way the channel pinch off region relocates. Yet the area under the curve, which is a measure for the total noise observed at the contacts, remains nearly the same when compared with the curve corresponding to $V_{ds} = V_{d,sat}$. As the electrons travel from the source and move toward the drain, the perpendicular field in the channel reduces approaching the pinch-off region. Since the density of electrons toward the pinch-off region is low when compared with the rest of the channel, the relative importance of number fluctuations increases resulting in higher noise

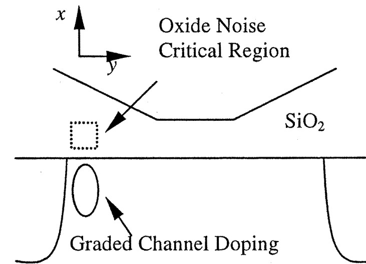

Fig. 7. Schematic device structure of a 45 μm graded n-channel MOS transistor.

contributions from the end of the channel as depicted. Both the Green's function and the local $g - r$ noise strength decrease as the electrons move beyond the pinch-off point, since the carriers move away from the interface, deeper into the substrate, thus reducing the probability of the carriers interacting with the traps in the oxide.

Simulation has shown that no significant difference in noise performance was found by switching the tunneling mechanism from the square barrier tunneling model to the trapezoidal tunneling model. The reason for this is that for the device under study with a gate oxide thickness of 89 Å, the effect of band bending at the locations where low frequency noise is generated is quite small.

The interface $g - r$ noise source, stemming from the carrier density fluctuations in the interface traps only, is negligible when compared with the velocity fluctuation or the oxide trapping noise. Thus the interface parameters, such as the interface capture coefficients c_n and c_p and the interface defect density $N_{T_{itf}}$, cannot be extracted from noise measurement data. The interface trap centers serve only as stepping-stones for the carriers in the channel to reach the trap centers in the oxide. The carrier transitions are limited by the carrier tunneling rates r_{ox} and g_{ox} defined in (13) and (14). Thus, the values of the interface parameters c_n and c_p and $N_{T_{itf}}$ do not affect the simulated oxide trapping noise outcome, as long as those parameters ensure that the carrier transition rates $r_{n,itf}$, $g_{n,itf}$, $r_{p,itf}$, and $g_{p,itf}$ are higher than the tunneling rates r_{ox} and g_{ox}. In the example shown in this section, we used 10^{-7} cm^3/s and 10^{11} cm^{-2} eV^{-1} for the interface capture coefficients and the interface defect density, respectively.

IV. Noise Spectroscopy

Motorola provided measured data of a production BiCMOS technology with an effective channel length of 0.25 μm [17]. A graded n-channel MOS (GCNMOS) transistor [18] with a geometric channel length of 0.45 μm was analyzed for this paper. This device has a gate oxide thickness of 50 Å, and a boron implant is present near the source region, as shown in Fig. 7. Both the device structure (such as the nonplaner oxide thickness) and the doping profile were calibrated through reverse engineering [19] of the measured I–V and C–V data. A prerequisite for accurate oxide trapping noise simulation is to have a dense grid point distribution in the oxide near the interface, since the characteristics of the noise components vary strongly with position. As mentioned previously, the interface parameters do not affect the oxide trapping noise outcome, as long as the interface carrier

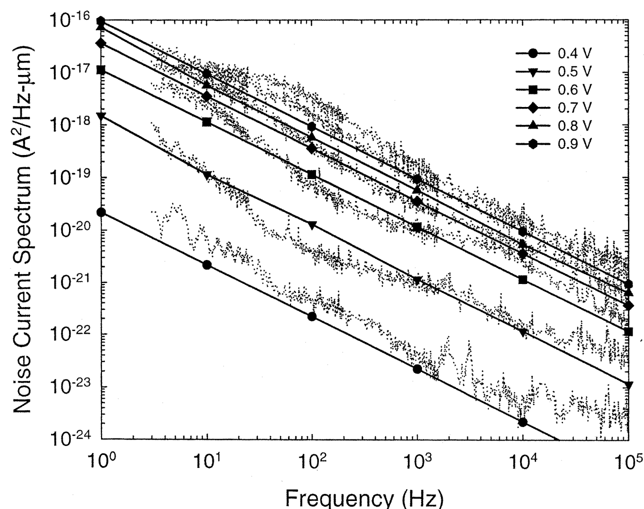

Fig. 8. Measured current noise spectral density as a function of V_{gs} and frequency. The drain bias V_{ds} is 2.0 V. The solid lines represent the simulated background $1/f$ noise components.

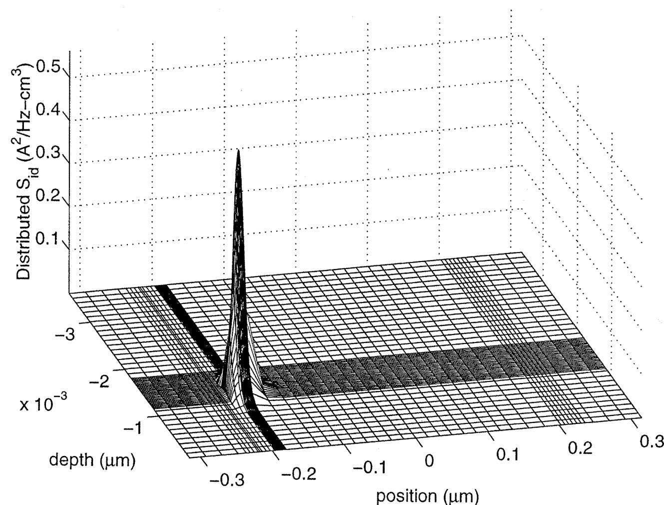

Fig. 9. Distributed current noise spectral density at $f = 25$ Hz. The bias values of the device under simulation are $V_{ds} = 2.0$ V and $V_{gs} = 0.8$ V. The oxide region is shown with $x = 0$ midway between the metallurgical source and drain junctions.

transition rates are faster than the carrier tunneling rates. Thus, for the GCMOS transistor under study the interface parameters for simulating the oxide trapping noise are set to default values of $c_n = c_p = 10^{-7}$ cm^3/s and $N_{0_{itf}} = 10^{11}$ cm^{-2} eV^{-1}. The defect density in the oxide is modeled according to (18), where the parameters are set to $\xi = 3.1$ eV^{-1} and $\eta = 0$. For the carrier-tunneling rate, the attenuation constant α is modeled by (21) instead of (20) for higher accuracy. The measured noise is plotted as dotted lines in Fig. 8. The data was taken at constant $V_{ds} = 2.0$ V and sweeping V_{gs} from 0.4 to 0.9 V. Since the threshold voltage V_t, extracted from both the measured and simulated I–V data, is 0.57 V, the measurements cover both the subthreshold and strong inversion modes of operation. To analyze the excess noise, each set of data for a specific gate bias voltage is decomposed into two parts: the background $1/f$ noise component, and the visible $g - r$ Lorentzian spectra.

To analyze the background $1/f$ component, simulations were carried out to find the value of N_0 that produces the best fit to the measured data. We discovered that for this device, the critical noise region is not located in the gate oxide above the center or near the drain region of the channel like in the example shown in Section III, but is located in the smile oxide directly above the graded channel boron implant near the source region, as the distributed current noise spectral density plotted in Fig. 9 illustrates. Even though the peak of the distributed noise moves horizontally (parallel to the y axis) with changing drain bias voltage and moves vertically (parallel to the x axis) for different frequency, the peak is always confined to the oxide area above the graded channel doping, indicated in Fig. 7. This phenomenon can be explained from a locally strong scalar Green's function coupling this particular noise region to the drain contact. The results of the simulations, presented as solid lines in Fig. 8, could only be generated by assuming a y-coordinate dependence of the parameter N_0 as shown in Fig. 10. Apparently the defect density required to generate the measured noise is higher where the smile oxide is thicker, as illustrated in Fig. 11. One possible explanation is that as the smile oxide gets thicker, increasing stress on the oxide generates more defect centers for

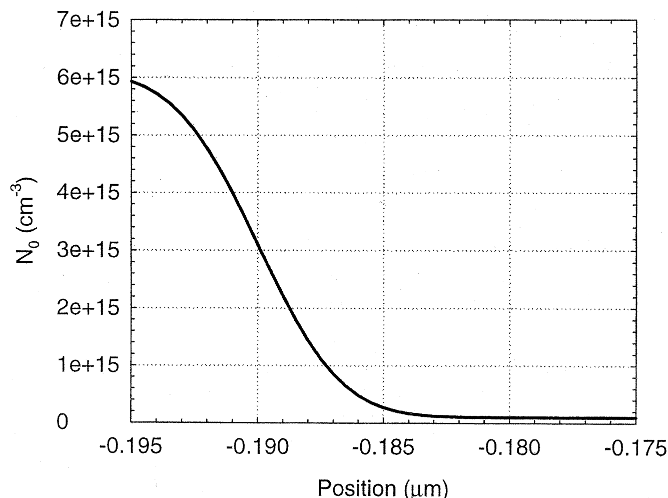

Fig. 10. Profile of the defect density parameter N_0 as function of position parallel to the channel. Note that the parameter is plotted only for the oxide noise critical region indicated in Fig. 7.

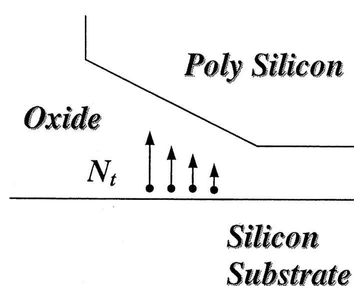

Fig. 11. Schematic defect density profile in the smile oxide.

the carriers to tunnel to from the interface. Another possible explanation maybe that in the formation of the graded channel by ion implantation through the poly gate and the smile oxide at a tilted angle, the oxide lattice structure in the smile oxide region is damaged creating the defect centers that produce the observed oxide trapping noise.

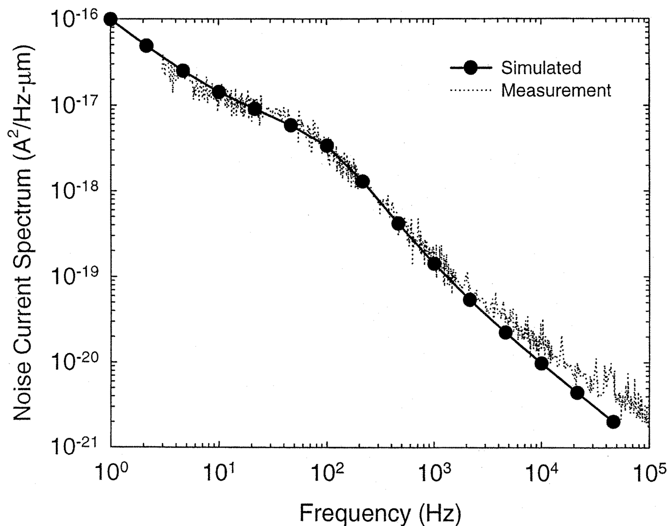

Fig. 12. Comparison of simulated and measured noise spectral densities at $V_{ds} = 2.0$ V and $V_{gs} = 0.9$ V. A single defect was simulated in a grid point 15 Å away from the interface producing the Lorentzian component observed in the simulated and measured data.

The Lorentzian spectra visible above the background $1/f$ noise may stem from pronounced defect distributions or single defects in the oxide. To test this hypothesis, a single defect is placed in the nodal volume at the grid point where the scalar Green's function shows a maximum at a frequency of 75 Hz, under the bias condition $V_{ds} = 2.0$ V and $V_{gs} = 0.9$ V. Note the good agreement between the simulation and the measured data shown in Fig. 12.

V. Summary

The implementation of oxide and interface trapping noise into a PDE-based simulator allows one to study the distribution of $1/f$-like noise sources in a MOSFET. Comparing measured and simulated noise data, the noise producing oxide defect densities can be determined. The oxide trapping noise simulator correctly predicts $1/f$-like noise spectral densities for MOS devices operating in subthreshold and strong inversion in saturation, regimes not accessible with analytical tools due to the two-dimensional complexity of the channel layout and carrier flow patterns.

Acknowledgment

The authors would like to thank R. Thoma, S. Banerjee, and B. Brown of the RF/IF Silicon Technology Development Department at the Motorola Digital DNA Labs for supplying us the doping profiles and the noise measurement data of the graded channel MOS devices. The Semiconductor Research Corporation supported this research.

References

[1] A. L. McWhorter, "$1/f$ noise and germanium surface properties," in *Semiconductor Surface Physics*, R. H. Kingston, Ed. Philadelphia, PA: Univ. of Pennsylvania Press, 1957, pp. 207–228.

[2] S. Christensson, I. Lundström, and C. Svensson, "Low frequency noise in MOS transistors-I theory," *Solid-State Electron.*, vol. 11, pp. 797–812, 1968.

[3] S. T. Hsu, D. J. Fitzgerald, and A. S. Grove, "Surface-state related $1/f$ noise in p–n junctions and MOS transistor," *Appl. Phys. Lett.*, vol. 12, pp. 287–289, May 1968.

[4] H.-S. Fu and C.-T. Sah, "Theory and experiments on surface $1/f$ noise," *IEEE Trans. Electron Devices*, vol. ED-19, pp. 273–285, Feb. 1972.

[5] Z. Celik and T. Y. Hsiang, "Study of $1/f$ noise in n-MOSFET's: Linear region," *IEEE Trans. Electron Devices*, vol. ED-32, pp. 2797–2802, Dec. 1985.

[6] F.-C. Hou, "Low-Frequency Bulk and Surface Generation-Recombination Noise Simulations of Semiconductor Devices," Ph.D. dissertation, Univ. Florida, Tallahassee, 2002.

[7] M. Liang and M. E. Law, "Influence of lattice self-heating and hot-carrier transport on device performance," *IEEE Trans. Electron Devices*, vol. 41, pp. 2391–2398, Dec. 1994.

[8] ——, "An object oriented approach to device simulation," *IEEE Trans. Computer-Aided Design*, vol. 13, pp. 1235–1240, Oct. 1994.

[9] E. Burstein and S. Lundquist, *Tunneling Phenomena in Solids*. New York: Plenum, 1969.

[10] M. Schulz, "Interface states at the SiO_2–Si interface," *Surf. Sci.*, vol. 132, pp. 422–455, 1983.

[11] Z. Celik-Butler and T. Y. Hsiang, "Spectral dependence of $1/f^{\gamma}$ noise on gate bias in n-MOSFET's," *Solid-State Electron.*, vol. 30, no. 4, pp. 419–423, 1987.

[12] C. T. Sah, "Theory of low-frequency generation noise in junction-gate field-effect transistors," *Proc. IEEE*, vol. 52, pp. 795–814, July 1964.

[13] F. P. Heiman and G. Warfield, "The effects of oxide traps on the MOS capacitance," *IEEE Trans. Electron Devices*, vol. ED-12, pp. 167–178, Apr. 1965.

[14] W.-C. Lee and C. Hu, "Modeling gate and substrate currents due to conduction- and valence-band electron and hole tunneling," in *2000 Symp. VLSI Technol. Dig. Tech. Papers*, 2000, pp. 198–199.

[15] E. Merzbacher, *Quantum Mechanics*. New York: Wiley, 1970.

[16] M. Depas, B. Vermeire, P. W. Mertens, R. L. Van Meirhaeghe, and M. M. Heyns, "Determination of tunneling parameters in ultra-thin oxide layer poly-Si/SiO_2/Si structures," *Solid-State Electron.*, vol. 38, pp. 1465–1471, 1995.

[17] F. K. Chai, C. S. Kyono, V. Ilderem, M. Kaneshiro, D. Zupac, S. Bigelow, C. Ramiah, P. Dahl, R. Braithwaite, D. Morgan, S. Hildreth, and G. Grynkewich, "A cost-effective 0.25 μm $L_{\rm eff}$ BiCMOS technology featuring graded-channel CMOS (GCMOS) and a quasiself-aligned (QSA) NPN for RF wireless applications," in *IEEE Bipolar Circuits Technology Meeting (BCTM)*, 2000, pp. 110–112.

[18] J. Ma, M.-B. Liang, R. A. Pryor, S. Cheng, M. H. Kaneshiro, C. S. Kyono, and K. Papworth, "Graded channel MOSFET for high performance, low voltage DSP applications," *IEEE Trans. VLSI Syst.*, vol. 5, no. 4, pp. 352–359, Dec. 1997.

[19] H. Goto, S. Yamaguchi, and C. Jungemann, "Inverse modeling as a basis for predictive device simulation of deep sub-micron MOSFET's," *Jpn. J. Appl. Phys*, vol. 37, pp. 5437–5443, 1998.

Fan-Chi Hou, photograph and biography not available at time of publication.

Gijs Bosman, photograph and biography not available at time of publication.

Mark E. Law (S'79–M'81–SM'92–F'98), photograph and biography not available at time of publication.